Received: 1 August 2022 | Revised: 8 September 2022 | Accepted: 9 September 2022

DOI: 10.1002/poc.4437

RESEARCH ARTICLE

Journal of Physical Organic Chemistry WILEY

Computational study on the reduction and solvolysis of triplet chlorobenzenes

Cristina Nitu[1,2] | **Stefano Crespi**[1]

[1]Department of Chemistry - Ångström Laboratory, Uppsala University, Uppsala, Sweden

[2]Stratingh Institute for Chemistry, Faculty of Mathematics and Natural Sciences, University of Groningen, Groningen, The Netherlands

Correspondence
Stefano Crespi, Department of Chemistry - Ångström Laboratory, Uppsala University, Box 523, 751 20 Uppsala, Sweden.
Email: stefano.crespi@kemi.uu.se

Funding information
Swedish Vetenskapsrådet, Grant/Award Number: 2021-05414; Swedish National Infrastructure for Computations (SNIC), Grant/Award Number: SNIC 2022/22-525

Abstract

In this work we explored the excited state reactivity of triplet chlorobenzenes with density functional theory and a cluster-continuum approach. We modeled two competing reactions: a direct abstraction of hydrogen from a solvent molecule and solvolysis via photo-S_N2Ar. Electron donating (–OMe, $–CH_2SiMe_3$, $–SiMe_3$) and withdrawing (–CN) substituents not only have distinct effects on the triplet geometries, inducing structural distortions due to the relief of excited state antiaromaticity, but also affect the reactivity of the system. Therefore, electron-rich chlorobenzenes favor the radical reduction, while electron deficiency opens the possibility for solvolysis. Both reactions are energetically comparable to or more favorable then the dissociation of the C-Cl bond to form triplet or singlet aryl cations, the intermediates considered responsible for these reactivities. Our findings can be correlated with experimental results on similar systems available from the literature, deeming the proposed pathways as viable alternatives to established mechanisms involving aryl cations.

KEYWORDS

density functional calculations, photochemistry, reduction, solvolysis, substituent effects

1 | INTRODUCTION

The population of an excited state by photochemical means alters the reactivity of an organic molecule, opening pathways that are unreachable in the ground state. Among all organic compounds, benzene and its derivatives represent a key example of this ground-excited state dichotomy. Indeed, benzene displays Hückel aromaticity in the S0 (owing to its 4n+2 π electrons), and it becomes antiaromatic in both multiplicities of its first excited state (S1 and T1), according to Baird's rule.[1–6]

The geometric and electronic alterations arising from excitation ultimately overturn the S0 reactivity rules of substituted benzenes and give rise to reactivities, which would be otherwise disfavored.[4,7,8] Taking halobenzenes as an example, the introduction of a halogen leads to the crossing of the first excited state π-π^* surface with the low lying π-σ^* of the bond between the carbon and the halogen.[4] Scission thus becomes possible from both the S1 and T1 states: the weaker the bond, the higher the photolysis quantum yield (I > Br > Cl).[4] Additional groups on the ring can affect the nature of the photodissociation channels through their relative position, inductive, conjugation, or steric effects.[9]

Among the halogenated compounds, the chloro-derivatives are particularly interesting from a synthetic

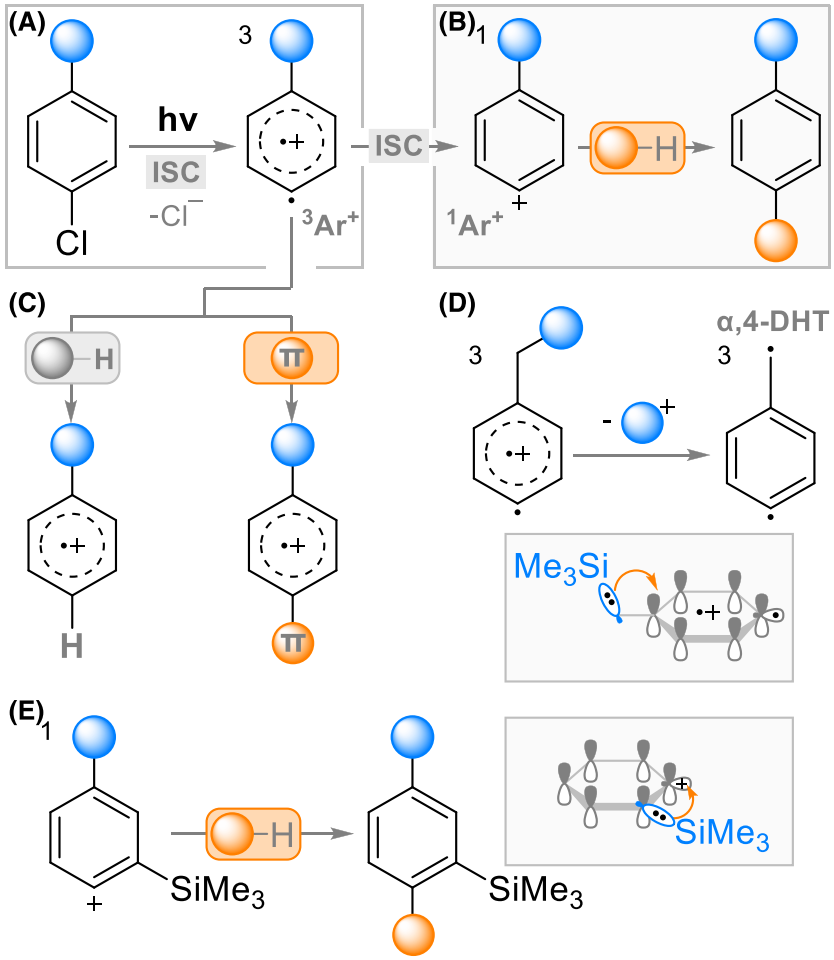

FIGURE 1 (A) Generation of triplet aryl cations from chloroarenes; (B) reactivity of singlet aryl cations: solvolysis; (C) reactivity of triplet aryl cations: reduction and attack of π-nucleophiles; (D) generation of didehydrotoluenes from triplet aryl cations. Box below: Orbital interactions arising from the β-silicon effect in triplet aryl cations. (E) Solvolysis of singlet aryl cations stabilized via the β-silicon effect. Box to the right: main orbital interactions

perspective, due to their propensity to undergo photochemical reactions with outcomes similar to the ground state S_N1Ar (photo-S_N1).[10,11] With electron-donating substituents (e.g., $-NR_2$ and –OR), the photolysis of aryl chlorides has been shown to lead to the reduction of arenes, namely, H abstraction, C-C bond formation with π nucleophiles or solvolysis products.[10,11] The current understanding of these reactions involves a mechanism on the triplet surface.[10–13] The dissociative T1 state is populated by excitation to the S1 followed by efficient intersystem crossing, or photosensitization (Figure 1A). The cleavage of the C-Cl bond generates a triplet cation intermediate stabilized by polar media (^{3}**Ar**$^+$, Figure 1A). The $\pi^5\sigma^1$ cation is eventually trapped with a π nucleophile, or it abstracts a hydrogen atom from its environment (Figure 1C), forming a radical cation that eventually rearomatizes via electron transfer. The cation can also populate its singlet (^{1}**Ar**$^+$, Figure 1B) with an efficiency dependent on the nature of its substituents,[13] leading to a closed shell singlet cation localized on the empty sp^2 orbital. This species is postulated to form solvolysis products (Figure 1B). The presence of other cleavable (electrofugal) groups in the structure, such as in chlorobenzyltrimethylsilanes or chlorobenzylphosphonates, opens up additional reaction pathways.[14–16] The second dissociation of the C-Si or C-P bond could happen at the triplet cation stage, triggered by the presence of a formal radical cation delocalized on the π orbitals (Figure 1D). A $\sigma\pi$ diradical species is consequently formed, namely, didehydrotoluene (**α,4-DHT** for the *para* derivative, in Figure 1D).[17–19] In contrast, a trimethylsilyl group placed in *ortho* to the chlorine induces a higher stabilization of the singlet phenyl cation compared to the triplet via the β-silicon effect (Figure 1E).[20] As a consequence, the reactivity of such systems is theorized to come from the singlet state leading preferentially to solvolysis products.[20]

The formation of the key intermediate ^{3}**Ar**$^+$ from the excitation of aryl chlorides has been postulated on the basis of transient spectroscopy data.[21–23] Nevertheless, the unequivocal presence of a triplet aryl cation ^{3}**Ar**$^+$ in solution in the photoreaction of chloroarenes remains elusive due to the spectral similarities with the radical cation resulting from the reaction of ^{3}**Ar**$^+$ with a nucleophile or the solvent (Figure 1C).[23] As a consequence, the triplet cation reactivity and selectivity has been

elucidated mainly via computational studies.[13,24–26] In these works, however, the interaction between the excited intermediate and a reagent, namely, a nucleophile or the solvent, was to the best of our knowledge studied at the singlet or triplet aryl cation stage and not starting from the triplet excited halobenzene precursor, in which the halogen cleavage is at its early stages.[27]

Analyzing the geometrical and electronic properties of triplet chlorobenzenes, we can hypothesize two types of reactivity for the undissociated triplet molecule. In order to relieve excited state antiaromaticity, C1 of the benzene ring puckers and/or the C-Cl bond bends outside the plane[6] (these distortions can be characterized through the definition of the proper dihedral α and the improper dihedral β in Figure 2A), exposing the triplet SOMO on the C1 carbon (Figure S1). The unpaired spin on C1 could potentially abstract a hydrogen from the solvent already at the C-Cl undissociated stage (Figure 2C), with

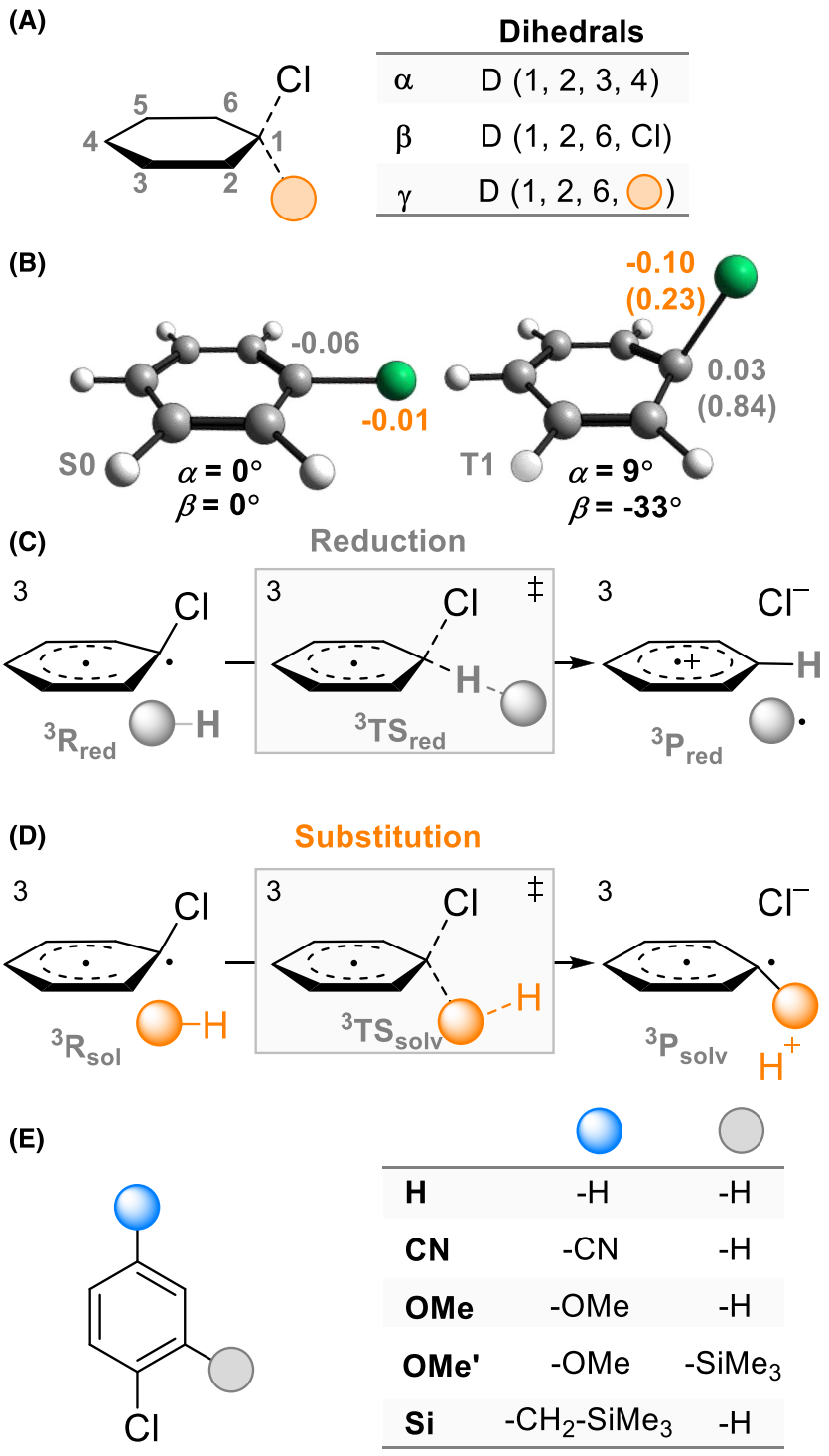

FIGURE 2 (A) Definition of proper and improper dihedrals for the characterization of ring puckering at C1 (α), out-of-plane bending of the C-Cl bond (β), and out-of-plane bending for a newly forming bond (γ). (B) Geometries of the S0 and T1 minima of chlorobenzene. Natural charges and spin (in brackets) for C1 (in gray) and Cl (in orange) are also provided and were obtained at the CPCM-(U)PWPBE95-D4/def2-QZVP//r^{2}SCAN-3c level; (C) proposed mechanisms for the reduction and (D) substitution (S_N2Ar) of triplet aryl chlorides; (E) compounds investigated in this work

concomitant loss of the chloride anion to form the dehalogenated radical, which will eventually lead to the reduced phenyl derivative after reductive electron transfer.

Moreover, the electrophilic site on the C1 carbon becomes accessible to the solvent or to other nucleophiles, enabling a substitution mechanism that resembles the single-step aliphatic S_N2 reaction, which would be otherwise impossible in the flat S0 structure (Figure 2D).[10] This hypothetical photo-S_N2Ar could also be favored by the build-up of positive charge on the ring predicted in polar solvents and more importantly by the increased polarization of the C-Cl bond (Figure 2B).[28] A third improper dihedral angle, namely, γ in Figure 2A, could be used to describe the trajectory of the two proposed mechanisms for the reduction and solvolysis at the triplet state.

The nature of the Ar-Cl substitution mechanism on the triplet surface poses a fundamental question related to the reactivity principles of excited aromatic molecules.[10,12,29] In this work, we explore computationally the possibility for a direct hydrogen atom abstraction (Figure 2C) and the photo-S_N2Ar mechanism (Figure 2D) in the photochemical solvolysis of differently substituted triplet aryl chlorides (Figure 2E), as an alternative to the more established mechanism involving the intermediacy of a 'naked' aryl cation.

2 | COMPUTATIONAL DETAILS

Density functional theory (DFT) optimization of minima and transition states, frequency, and single-point calculations were carried out with the ORCA 5.0.3 quantum chemical package,[30,31] while xTB was used for semiempirical tight-binding methods at the GFN2-xTB level.[32,33] The CREST utility of xTB 6.5.0 in combination with the Quantum Cluster Growth (QCG) algorithm was used for the addition of three explicit methanol molecules to the optimized transition state geometries, while keeping the solute fixed.[34–36] Three solvent molecules were the minimal that allowed for stabilization of the solvolysis transition state and product, by the formation of a cluster where the chloride and a proton are exchanged. The geometry for the reduction cluster is slightly different from the solvolysis one because only one molecule stabilizes Cl^- as an anion while the third one interacts with the reactive MeOH that donates the hydrogen atom. The different arrangement is due to the different nature of the reactions, however, all the molecules play a role in the stabilization of either the chloride or the other intermediates formed.

Calculations were performed both in gas phase and with methanol as implicit solvent within the conductor-like continuum polarizable model (CPCM).[37] Complete active space self-consistent field (CASSCF) optimizations were performed with OpenMolcas 20.10,[38,39] with an (8,8) active space consisting of 3 π, 3 π^*, 1 $\sigma_{C\text{-}Cl}$, and 1 $\sigma^*_{C\text{-}Cl}$ orbitals. Natural bond orbital analysis was done with NBO 6.0.[40]

A benchmark study for C-Cl bond lengths and improper dihedral angles was carried on singlet (S0) and triplet (T1) chlorobenzene, using the following methods for optimization in the gas phase: (U)B3LYP/6-311+G(2d,p),[41–43] (U)B3LYP/def2-TZVP,[41,42,44,45] M06-2X-D3 (zero damping)/def2-TZVP,[44–47] r^2SCAN-3c,[48] SA2-CASSCF(8,8)/def2-TZVP,[44,49,50] and GFN2-xTB.[33] Electronic energies were corrected with (U)PWPBE95-D4/def2-QZVP[44,45,51,52] single point calculations that were also used to obtain natural charges and spin populations via NBO analysis.

The hydrogen atom abstraction (reduction) and solvolysis on the triplet surface of differently substituted chlorobenzenes (Figure 2) were characterized in three steps, both in the gas phase and with implicit solvation:

2.1 | Transition states with three solvent molecules

After individual pre-optimization with GFN2-xTB (only in gas phase), triplet minima were used to form clusters with three methanol molecules. The clusters were optimized as triplet transition states with xTB and used for subsequent optimization with the composite method r^2SCAN-3c (from now on both in gas and implicit solvent phase). Only one imaginary frequency was obtained for each r^2SCAN-3c transition state.

2.2 | Reactants and products

Preliminary geometries for reactants and products were obtained from distortion of each transition state along the respective imaginary mode. These were optimized as triplet minima with r^2SCAN-3c. Lastly, the triplet reactants were optimized as ground state singlets with r^2SCAN-3c.

2.3 | Energies, natural atomic charges, and spin populations

(U)PWPBE95-D4/def2-QZVP single point calculations were performed on all the optimized transition states and minimum geometries. Natural atomic charges and spin populations were extracted from NBO analysis, while

Gibbs free energy corrections from r^{2}SCAN-3c frequency calculations.

3 | RESULTS AND DISCUSSION

3.1 | Benchmark

Substituent effects on the generation of aryl cations from triplet aryl chlorides and on their reactivity have been commonly investigated with the (U)B3LYP functional and a Pople basis set such as 6-311+G(2d,p).[6,28] However, the analysis of the systems was limited to implicit solvation in the vast majority of the examples present in the literature. The incorporation of explicit solvent molecules using a cluster-continuum approach[53] could aid in the stabilization of the intermediates and in the better description of the underlying mechanism, starting already from the undissociated C-Cl bond in the triplet excited state of chlorobenzenes. Such an approach comes with the drawback of increased computational cost, due to the larger number of degrees of freedom to be computed. In order to determine whether reliable geometries can be obtained from more modern and inexpensive methods, a benchmark study was conducted by optimizing the ground and excited triplet states of chlorobenzene (see Table 1 for the triplet states and Table S1 for the ground state singlets). On top of the optimizations, we performed NBO analysis and single point calculations at the CPCM-PW6B95-D4/def2-QZVP level.[54] As can be seen in Tables 1 and S1, changing only the basis set from the established optimization method to def2-TZVP yielded S0 and T1 structures with minimal differences from 6-311+G(2d,p). Another functional previously employed for aryl cations, namely, M06-2X, resulted in a shortening of the C-Cl bond for both states.[55] The partial charges at the triplet stage differed from (U)B3LYP/6-311+G(2d,p), with a charge underestimation at Cl and a negative sign at the *ipso* carbon. Next, the r^{2}SCAN-3c geometries were similar to the (U)B3LYP/6-311+G(2d,p) references in terms of the C-Cl bonds, atomic charges, and spins, while the triplet ring puckering was more pronounced. Judging from the RMSD, the composite method r^{2}SCAN-3c was therefore comparable with (U)B3LYP/def2-TZVP at the ground state and with M06-2X-D3 at the triplet state, but at a lower computational cost. CASSCF resulted in the most structural distortions from the (U)B3LYP/6-311+G(2d,p) reference for the T1 geometry: shorter C-Cl, less ring puckering and the highest RMSD value among the methods considered. The ground state CASSCF structure was also dissimilar from the corresponding reference, with a relatively high RMSD, a longer C-Cl and partial charge underestimation at both Cl and the *ipso* carbon. Lastly, GFN2-xTB also gave shorter C-Cl bonds, along with a higher degree of ring puckering of the triplet. Interestingly, this semiempirical method performed reasonably for the triplet geometry based on the low RMSD, even though it was the worst for the ground state.

Given the acceptable triplet geometry optimized with GFN2-xTB in the benchmark study, the method was used in the pre-optimization of chlorobenzene triplet transition states in the presence of three methanol molecules. The results for the two reactions considered, reduction and solvolysis, can be seen in the supporting information (Table S2). We decided to adopt r^{2}SCAN-3c for the geometry optimizations owing to the good performances in terms of RMSD and the overall computational cost. Consequently, the GFN2-xTB structures were used as starting points for the r^{2}SCAN-3c optimization for all

TABLE 1 Benchmark study of the triplet chlorobenzene, optimized at various levels of theory in gas phase

	T1 state						
	C-Cl (Å)	α[b] (deg)	Cl charge[c]	C1 charge[c]	Cl spin[c]	C1 spin[c]	RMSD[d] *10^{-2}
(U)B3LYP/6-311+G(2d,p)	1.83	8.6	−0.09	0.02	0.22	0.84	0.0
(U)B3LYP/def2-TZVP	1.81	8.6	−0.07	0.00	0.22	0.83	0.7
(U)M06-2X-D3[a]/def2-TZVP	1.77	9.3	−0.03	−0.02	0.21	0.83	2.7
(U)r^{2}SCAN-3c	1.84	9.3	−0.10	0.03	0.23	0.84	2.8
GFN2-xTB	1.79	9.8	−0.06	0.00	0.23	0.83	3.5
SA2-CASSCF(8,8)/def2-TZVP	1.80	7.2	−0.06	0.00	0.21	0.83	5.2

[a]D3 dispersion correction with zero damping.[47]

[b]Dihedral angle characterizing ring puckering at C1, as defined in Figure 2A.

[c]Charges and spin populations derived from NBO analysis and CPCM-PW6B95-D4/def2-QZVP single point calculations.

[d]RMSD values reported relative to the T1 geometry optimized at the (U)B3LYP/6-311+G(2d,p) level in gas phase.

the chlorobenzene derivatives (Figure 2E). In the case of **Si** we considered two conformers at the triplet excited state, namely, the one with the C-Cl bond and the $-CH_2$-$SiMe_3$ substituent pointing in the same side (**Si(Z)**) or in the opposite sides (**Si(E)**) of the ring. For all compounds, we considered four species in the presence of three methanol molecules for each reaction: ground state reactant (**R**), triplet reactant (^{3}**R**), triplet transition state (^{3}**TS**), and triplet product (^{3}**P**). The structures are referred to in the text by labels containing the substituent *para* to the chlorine, the species concerned and the type of reaction—**red** for reduction or **solv** for solvolysis—as subscript. For instance, **OMe-^{3}P$_{solv}$** corresponds to the triplet solvolysis product of *p*-methoxy-chlorobenzene.

3.2 | Triplet chlorobenzenes

The structural parameters, NBO atomic charges and spins and relative Gibbs energies obtained from calculations with CPCM (methanol) are listed in Tables 2 and 3; gas phase results are shown in the supporting information (Tables S3 and S4). It is noteworthy that the pairs **R$_{red}$/R$_{solv}$** and ^{3}**R$_{red}$/^{3}R$_{solv}$** correspond to the same species, but they were generated by distorting different transitions states characterized by distinct arrangements of explicit methanol molecules (**TS$_{red}$** for **R$_{red}$** and ^{3}**R$_{red}$**, while **TS$_{solv}$** for **R$_{solv}$** and ^{3}**R$_{solv}$**); for this reason, we observed slight differences between their structural and NBO properties.

TABLE 2 Structural parameters, natural atomic charges, spin populations, and relative Gibbs free energies for the ground state and triplet geometries modeled for the reduction of aryl chlorides optimized with CPCM-r^{2}SCAN-3c

		Reduction									
		C-Cl (Å)	C-H (Å)	α[a] (deg)	β[a] (deg)	γ[a] (deg)	Cl charge[b]	C1 charge[b]	Cl spin[b]	C1 spin[b]	ΔG[c] (kcal/mol)
H	**R$_{red}$**	1.77		0.2	−0.3		−0.02	−0.06			−80.4
	^{3}**R$_{red}$**	2.43		2.5	−48.5		−0.51	0.27	0.37	0.97	0.0
	^{3}**TS$_{red}$**	2.43	1.58	2.2	−49.8	19.3	−0.49	0.13	0.40	0.79	5.0
	^{3}**P$_{red}$**		1.08				−0.45	−0.11	0.46	0.16	−16.6
CN	**R$_{red}$**	1.75		−0.2	−0.1		0.02	−0.03			−73.7
	^{3}**R$_{red}$**	1.73		1.1	−1.6		0.07	−0.05	0.11	0.61	0.0
	^{3}**TS$_{red}$**	1.94	1.49	3.3	−38.5	33.5	−0.17	−0.09	0.20	0.52	9.9
	^{3}**P$_{red}$**		1.08				−0.41	−0.10	0.50	0.11	−8.3
OMe	**R$_{red}$**	1.76		0.1	−0.1		−0.01	−0.10			−71.8
	^{3}**R$_{red}$**	2.57		3.1	−48.9		−0.65	0.32	0.26	1.11	0.0
	^{3}**TS$_{red}$**	2.68	1.58	1.0	−54.1	13.3	−0.69	0.19	0.24	0.92	5.0
	^{3}**P$_{red}$**		1.08				−0.78	−0.02	0.14	0.33	−17.0
OMe′	**R$_{red}$**	1.77		−0.1	−0.4		−0.02	−0.06			−70.1
	^{3}**R$_{red}$**	2.67		4.4	−56.9		−0.68	0.33	0.24	1.16	0.0
	^{3}**TS$_{red}$**	2.93	1.54	2.0	−66.0	2.6	−0.78	0.20	0.16	0.94	4.4
	^{3}**P$_{red}$**		1.09				−0.75	−0.03	0.17	0.33	−15.9
Si(Z)	**R$_{red}$**	1.77		−0.1	−0.2		−0.03	−0.07			−70.9
	^{3}**R$_{red}$**	2.51		6.1	−45.6		−0.63	0.28	0.27	1.10	0.0
	^{3}**TS$_{red}$**	2.63	1.51	1.4	−50.7	15.3	−0.66	0.14	0.26	0.86	5.9
	^{3}**P$_{red}$**		1.09				−0.73	−0.04	0.19	0.30	−15.2
Si(E)	**R$_{red}$**	1.76		−0.1	−1.0		−0.02	−0.07			−71.4
	^{3}**R$_{red}$**	2.55		3.3	−47.8		−0.65	0.29	0.26	1.11	0.0
	^{3}**TS$_{red}$**	2.70	1.53	2.3	−53.9	12.6	−0.70	0.16	0.23	0.89	5.1
	^{3}**P$_{red}$**		1.09				−0.76	−0.04	0.16	0.31	−15.9

[a]Dihedral angles as defined in Figure 2A.
[b]Values derived from NBO analysis and CPCM-PW6B95-D4/def2-QZVP single point calculations.
[c]Electronic energies from CPCM-PW6B95-D4/def2-QZVP single point calculations and Gibbs corrections from CPCM-r^{2}SCAN-3c frequency calculations.

TABLE 3 Structural parameters, natural atomic charges, spin populations, and relative Gibbs free energies for the ground state and triplet geometries modeled for the solvolysis of aryl chlorides optimized with CPCM-r^{2}SCAN-3c

		Solvolysis									
		C-Cl (Å)	C-O (Å)	α[a] (deg)	β[a] (deg)	γ[a] (deg)	Cl charge[b]	C1 charge[b]	Cl spin[b]	C1 spin[b]	ΔG[c] (kcal/mol)
H	$\mathbf{R_{solv}}$	1.76		0.1	−0.1		−0.02	−0.05			−79.7
	$^3\mathbf{R_{solv}}$	2.43		2.7	−49.8		−0.52	0.27	0.37	0.97	0.0
	$^3\mathbf{TS_{solv}}$	2.80	1.71	−5.6	−65.9	37.7	−0.75	0.33	0.18	0.87	7.8
	$^3\mathbf{P_{solv}}$		1.41				−0.83	0.23	0.01	0.79	−4.1
CN	$\mathbf{R_{solv}}$	1.75		0.0	−0.1		0.02	−0.03			−73.7
	$^3\mathbf{R_{solv}}$	1.73		1.2	−0.7		0.06	−0.05	0.10	0.62	0.0
	$^3\mathbf{TS_{solv}}$	2.61	1.84	−2.5	−63.9	42.2	−0.60	0.28	0.33	0.82	14.0
	$^3\mathbf{P_{solv}}$		1.36				−0.82	0.27	0.00	0.52	−9.5
OMe	$\mathbf{R_{solv}}$	1.77		0.2	0.0		−0.03	−0.08			−70.7
	$^3\mathbf{R_{solv}}$	2.50		3.3	−43.8		−0.62	0.28	0.28	1.07	0.0
	$^3\mathbf{TS_{solv}}$	3.11	1.66	−7.9	−62.0	34.4	−0.87	0.35	0.07	0.92	11.2
	$^3\mathbf{P_{solv}}$		1.42				−0.84	0.24	0.00	0.81	−0.7
OMe′	$\mathbf{R_{solv}}$	1.78		0.0	−0.4		−0.04	−0.06			−67.4
	$^3\mathbf{R_{solv}}$	2.57		4.1	−47.5		−0.65	0.33	0.27	1.09	0.0
	$^3\mathbf{TS_{solv}}$	3.39	1.68	−8.9	−71.9	34.9	−0.91	0.38	0.03	0.94	11.5
	$^3\mathbf{P_{solv}}$		1.42				−0.85	0.30	0.00	0.85	2.4
Si(Z)	$\mathbf{R_{solv}}$	1.77		−0.1	0.3		−0.03	−0.07			−71.4
	$^3\mathbf{R_{solv}}$	2.52		6.1	−45.4		−0.63	0.30	0.28	1.06	0.0
	$^3\mathbf{TS_{solv}}$	3.05	1.67	−6.4	−64.9	35.3	−0.86	0.35	0.08	0.91	11.3
	$^3\mathbf{P_{solv}}$		1.42				−0.84	0.23	0.00	0.79	1.2
Si(E)	$\mathbf{R_{solv}}$	1.77		−0.1	−0.1		−0.04	−0.24			−72.2
	$^3\mathbf{R_{solv}}$	2.55		3.3	−46.6		−0.65	0.31	0.26	1.07	0.0
	$^3\mathbf{TS_{solv}}$	3.07	1.68	−5.0	−64.7	35.2	−0.86	0.35	0.07	0.91	9.7
	$^3\mathbf{P_{solv}}$		1.41				−0.85	0.24	0.00	0.80	−2.1

[a]Dihedral angles as defined in Figure 2A.
[b]Values derived from NBO analysis and CPCM-PW6B95-D4/def2-QZVP single point calculations.
[c]Electronic energies from CPCM-PW6B95-D4/def2-QZVP single point calculations and Gibbs corrections from CPCM-r^{2}SCAN-3c frequency calculations.

The optimized singlet reactant geometries were planar with C-Cl bond lengths consistent across all compounds considered, as expected for ground state chlorobenzenes. The triplet reactants presented distortions depending on the nature of the substituents. We can consider **H-^{3}R** as an illustrative example, where the longer C-Cl distance compared to the ground state, puckering at C1 and out-of-plane bending of the C-Cl bond alleviate the antiaromatic character of the triplet benzene ring (α increases from 0.2 to 2.5° and β from −0.3 to −48.5°, Table 2).[6] Consequently, C-Cl becomes more polarized with build-up of partial negative charge on Cl and positive on C1.[28] The effect of solvation on the ring puckering and C-Cl distance is evident. The ring puckering in the optimized structures of **H-^{3}R** increases following the series *cluster-continuum*[53] *(three MeOH with CPCM) < cluster (three MeOH in gas phase) < no solvation* ($\alpha = 2.5° < 4.2° < 9.3°$, considering the reduction path, see Figure 3 and Tables 1, 2, and S3), while the C-Cl bond distance follows the opposite trend (2.43 > 2.30 > 1.84 Å). This effect is consistent with a greater stabilization of the opposite charges on the Cl (partially negative) and on the ring (partially positive), which favors a heterolytic bond scission in polar protic media and a decreased interaction between the halogen and the ring. As expected, one of the two unpaired triplet spins is mostly localized at the C1 on the orbital that will eventually form the sp^2 hybridized σ radical of **^{3}Ar$^+$** (see Figures 1 and S1). The second one is partially delocalized on the ring and on the chlorine (see Tables 1–3 and

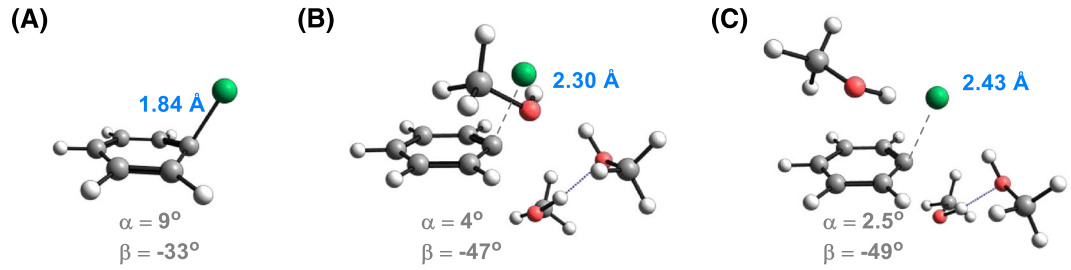

FIGURE 3 Triplet chlorobenzene structures with corresponding C-Cl distance (in blue), puckering dihedral (α), and C-Cl out-of-plane bending improper dihedral (β) optimized at the r^{2}SCAN-3c level with (A) no solvation; (B) with three explicit methanol molecules; (C) with three explicit methanol molecules and implicit solvation with conductor-like continuum polarizable model (CPCM) (methanol)

Figure S1). The introduction of an electron-donor *para* to the chlorine increased the C-Cl distance and polarization in the order **H-^{3}R** < **Si(Z)-^{3}R** < **Si(E)-^{3}R** < **OMe-^{3}R**, while two such substituents in *ortho* and *para* positions (i.e., **OMe′-^{3}R**) led to an even longer C-Cl and higher partial charges. The electron donating substituents also cause a partial shift of spin population from Cl to C1, suggesting that an enhanced electron donation to the ring promotes the heterolytic dissociation of Cl as a closed shell anion.[28] The resulting fragments still interact with each other as seen from the respective SOMOs (Figures S3–S6). If the C-Cl bond was fully dissociated, the ring would be flat as in a triplet aryl cation. Nevertheless, the puckering of the triplet reactants **Si(Z)-^{3}R, Si(E)-^{3}R, OMe-^{3}R,** and **OMe′-^{3}R** is more pronounced than the one for **H-^{3}R**, while their Cl spin populations are non-zero (0.24–0.37) and the Cl charges lower than unity (−0.62 to −0.68). The structures could be thus considered in the first stages of bond dissociation, still maintaining a directional interaction between the carbon and the chlorine.

In contrast, the triplet **CN-^{3}R** closely resembles the ground state **CN-R**, when optimized with implicit solvation, apart from the slight compression of the C-Cl distance by 0.02 Å and minimal out-of-plane C-Cl bending (0.7–1.6 Å) and ring puckering (∼1°). The interaction of the CN substituent is extremely relevant, as it can be seen by the diminished C–CN bond distance going from the S0 (1.42 Å) to the T1 (1.38 Å) and the elongation of the triple bond (from 1.16 to 1.18 Å). The spin population in this case is more delocalized on the ring (Table S5) due to the electron withdrawing nature of the –CN group, resulting in lower Cl and C1 spins compared to **H-^{3}R**. Consequently, –CN reduced the unpaired π spin density on the ring[6] relieving the triplet antiaromaticity without large geometrical distortions. As a side note, the gas phase **CN-^{3}R** geometry has a more pronounced C-Cl out-of-plane bending (Tables S3 and S4), indicating that the polarizable medium from the CPCM calculations also played a role in the stabilization of the antiaromatic planar structure.

3.3 | Reduction

We modeled the transition states for the hydrogen abstraction by triplet chlorobenzenes according to the mechanism proposed in Figure 2B (see also Table 2 and Figures 4 and S2–S6). In the case of unsubstituted chlorobenzene, **H-^{3}TS$_{red}$** maintains the characteristics of the triplet reactant, more specifically the puckering at C1, the C-Cl out-of-plane bending and the C-Cl distance. The hydrogen atom donor, that is, a methanol molecule, approaches C1 from the opposite side of the ring relative to the C-Cl bending (the improper dihedral $\gamma = 19.3°$, indicating the angle of approach of the H, with opposite sign of the Cl bending dihedral $\beta = -49.8°$ in Table 2). The relatively low γ angle evidences the direct interaction of H with the SOMO lobe of the triplet chlorobenzene on C1 (Figure 5). The absolute value of the partial charge on Cl decreases along the reaction coordinate (from −0.51 to −0.45). At the same time, the Cl spin increases going from **H-^{3}R$_{red}$** to **H-^{3}TS$_{red}$** then **H-^{3}P$_{red}$** (0.37 to 0.40 then 0.46), suggesting also a partial homolytic component in the dissociation in the unsubstituted chlorobenzene. The large reduction in the spin on C1 along the reduction confirms the radical nature of the hydrogen abstraction, leaving the benzene ring in **H-^{3}P$_{red}$** as a radical cation.

The nature of the C-Cl cleavage could be shifted toward pure heterolysis while still keeping the radical character of the reduction by introducing electron donating groups on the ring. According to the evolution of the charges and spins during the reduction of triplet **Si(Z), Si(E), OMe,** and **OMe′**, all of them undergo heterolytic dissociation as the Cl charge has a substantial rise and the Cl spin drops (Table 2).[28] As opposed to chlorobenzene, **OMe-^{3}TS$_{red}$, Si(Z)-^{3}TS$_{red}$** and **Si(E)-^{3}TS$_{red}$** have C-Cl distances longer by 0.11–0.15 Å compared to their

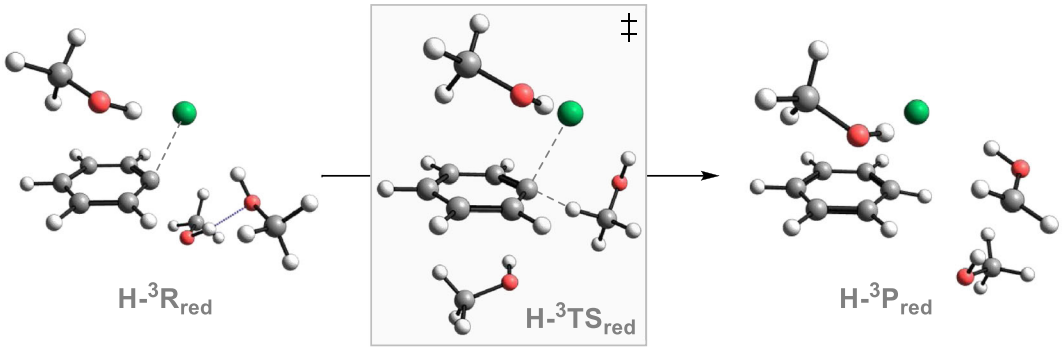

FIGURE 4 Optimized triplet reactants, transition states, and triplet products (CPCM-r^{2}SCAN-3c) for the reduction of chlorobenzene

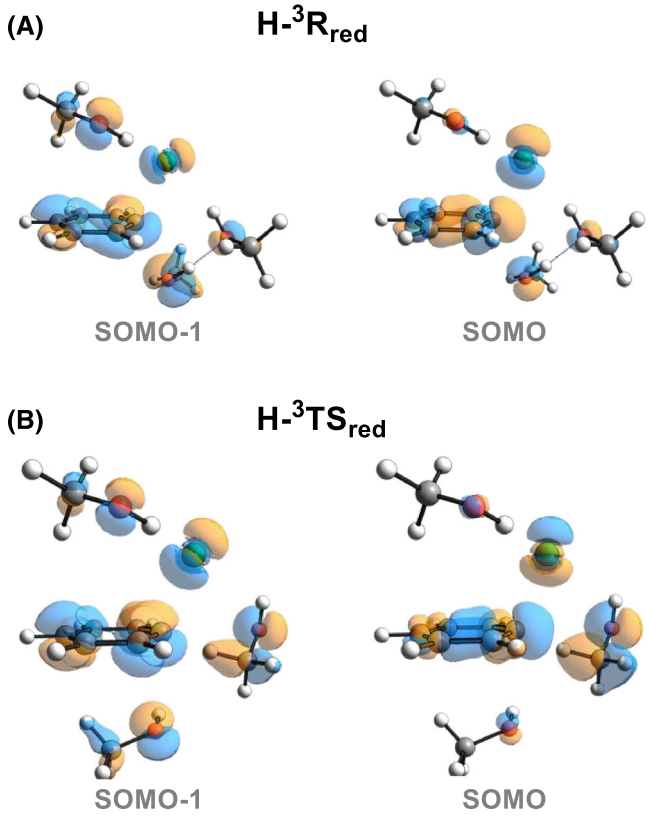

FIGURE 5 Singly occupied molecular orbitals (SOMO and SOMO-1) of the triplet reactants (A) and transition state (B) for the reduction of chlorobenzene (isovalue = 0.03, CPCM-(U) PWPBE95-D4/def2-QZVP//r^{2}SCAN-3c)

respective triplet reactants and the ring puckering (α in Table 2) is diminished. The extended degree of C-Cl dissociation in these structures is reflected also in the C1 and Cl partial charges, which are higher than in **H-^{3}TS$_{red}$**. The transition states with one electron donating substituent thus start to resemble triplet aryl cations as the rings flattened bringing the exposed SOMO lobe into the plane of the ring. Consequently, the methanol molecule has a different orientation relative to ring (i.e., γ between 12.6° and 15.3°, lower than **H-^{3}TS$_{red}$**). With its two electron donating groups, **OMe′-^{3}TS$_{red}$** represents an extreme case: the hydrogen undergoing abstraction is almost coplanar with the ring (2.6° vs. 13.3 of **MeO-^{3}TS$_{red}$**), while the Cl spin is low (0.16) and the Cl charge is the highest among all transition states (−0.78). A complete heterolytic dissociation has possibly already taken place at this stage, promoted by the electron richness of the benzene ring. The charges and spins of **OMe′-^{3}TS$_{red}$** resemble its product more than its precursor, indicating a late transition state.

Placing an electron acceptor group *para* to the chlorine had an opposite effect on the transition state geometry. The structure of **CN-^{3}TS$_{red}$** lost the planarity associated with its triplet reactant, puckering at C1 and bending the C-Cl out of the plane ($\alpha = 3.3°$ and $\beta = -38.5°$, Table 2). The higher ring distortion of **CN-^{3}TS$_{red}$** compared to **H-^{3}TS$_{red}$** affected the SOMO and consequently the orientation of the hydrogen atom relative to the benzene ring, as the γ improper dihedral widened (33.5° vs. 19.3°). Lastly, the C-Cl dissociation for this case has partial homolytic contributions, since the charges and spins of **CN-^{3}P$_{red}$** are similar to **H-^{3}P$_{red}$**.

Energetically, the reduction of triplet chlorobenzene is comparable to its derivatives containing electron-donating groups, with activation energies of 4.4–5.9 kcal/mol and **ΔG$_{red}$** between −17.0 and −15.2 kcal/mol. For **CN** the barrier is almost double (9.9 kcal/mol), due to its higher spin delocalization (and consequently lower spin population at C1). **ΔG$_{red}$** for **CN** is also less favorable than for the other compounds (−8.3 kcal/mol) due to the electron withdrawing substituent having a destabilizing effect on the radical cation product. Considering just the dissociation of triplet chlorobenzenes with similar substituents in the *para* position, the barriers computed in previous research at the CPCM-UB3LYP/6-311+G(2d,p) level for C-Cl stretching range from 9.5 and 10.6 kcal/mol for *p*-CH_2SiMe_3 and *p*-OMe, to 18.6 kcal/mol for chlorobenzene and 52.6 kcal/mol for *p*-NO_2.[28] The

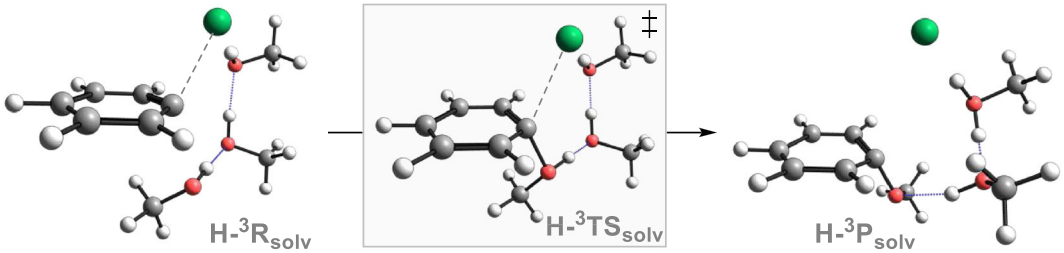

FIGURE 6 Optimized triplet reactants, transition states, and triplet products (CPCM-r^{2}SCAN-3c) for the solvolysis of chlorobenzene

activations energies for the direct radical hydrogen abstraction by undissociated triplet chlorobenzenes from this study are therefore comparable to or even lower than the generation of the triplet aryl cation. This comparison is derived from different theoretical models and consequently can be considered semi-quantitative at most; nevertheless, it supports the formation of reduction products via the triplet surface as a possible alternative pathway to be considered together with the aryl cation hypothesis.

On another note, the barrier for C-Si dissociation from the triplet *p*-CH_2SiMe_3 phenyl cation was previously found as 20.3 kcal/mol (CPCM-CASSCF(10,10)/6-31G(d)).[14] It is highly unlikely that the C-Si bond cleavage could precede the reduction of the triplet chloroderivative even in polar protic environment, if the triplet surface is populated. Indeed, the lifetime of the Ar-CH_2SiMe_3 radical cations (a species that mimics the electronic interactions between the silyl substituent and the ring comparable to ^{3}**Ar**$^+$ of **Si**) in HFIP solution was found to be 14 μs.[56] Even considering a nucleophile/solvent-assisted mechanism, the lifetime of the same silylated radical cation is 56 ns,[56] which is considerably longer than the one of the σ unpaired spin of the triplet aryl cations, which have a lifetime as short as <15 ps in solution.[21] Hence, it is challenging that the strong C-Si bond dissociates before the unpaired spin on C1 reacts with its environment. Thus, both these computational results and the experimental lifetimes may not support the photochemical formation of **DHTs** in solution.[19]

3.4 | Solvolysis

Photo-S_N2Ar mechanisms have already been formulated in literature, often involving the formation of a Meisenheimer complex in the excited state.[57–60] Such a reactivity seen, for instance, in the substitution of –NO_2 by ethyl glycinate in *p*-nitroanisole parallels the ground state nucleophilic aromatic substitution via consecutive addition-elimination processes.[61] In this work, we modeled the transition states for the theorized photo-S_N2Ar solvolysis on the triplet surface (Figure 2D) in which the leaving group departure and the nucleophilic attack happen concomitantly (Table 3 and Figures 6 and S2–S6). This mechanism resembles the aliphatic S_N2 reaction, and it is made possible by the distortions of the ring at the electrophilic site driven by the antiaromaticity relief on the triplet surface.

Returning to the example of unsubstituted chlorobenzene, in **H-^{3}TS$_{solv}$** the nucleophile (i.e., alcohol group of one explicit methanol molecule) approaches C1 from the side opposite to the C-Cl bending (i.e., negative $\beta = -65.9°$ and positive $\gamma = 37.7°$ in Table 3), similarly to the previous reaction. The nucleophile is, however, oriented relative to the plane of the ring at a wider angle than the hydrogen atom in **H-^{3}TS$_{red}$** (γ as 37.7° vs. 19.3°), indicating that different orbitals of the triplet chlorobenzene are involved in the reduction and the solvolysis (see Figures 5 and 7). For the reduction, the molecular orbital of the ring abstracting the hydrogen from the methanol has a larger sp^2 component on C1, while for the solvolysis the nucleophile interacts with an MO with a larger π character. This difference not only explains the angle of approach for the H and the nucleophile but is at the core of the Janus reactivity that we propose for the triplet chlorobenzenes.

As a consequence of the nucleophilic attack, the C-Cl distance becomes longer by 0.37 Å and the ring puckering changes direction from the Cl side to the O side, a change reflected in the sign of the α dihedral in **H-^{3}R$_{solv}$** (2.7°) versus **H-^{3}TS$_{solv}$** (−5.1°). The C-Cl bond in **H-^{3}TS$_{solv}$** is thus mainly dissociated, supported by the large increase in Cl and C1 partial charges (−0.75 and 0.33, respectively). At the transition state, the bond between C-O is only partially formed (1.71 Å), while the methanol proton is still attached to the oxygen. The C-Cl cleavage renders an even higher Cl charge (−0.83) in **H-^{3}P$_{solv}$** and a Cl spin population of only 0.1, evidencing the heterolytic nature of the process. Simultaneously, the proton detaches from the methanol nucleophile and is transferred to the other explicit solvent molecules forming a small hydrogen-bonded network, which interacts

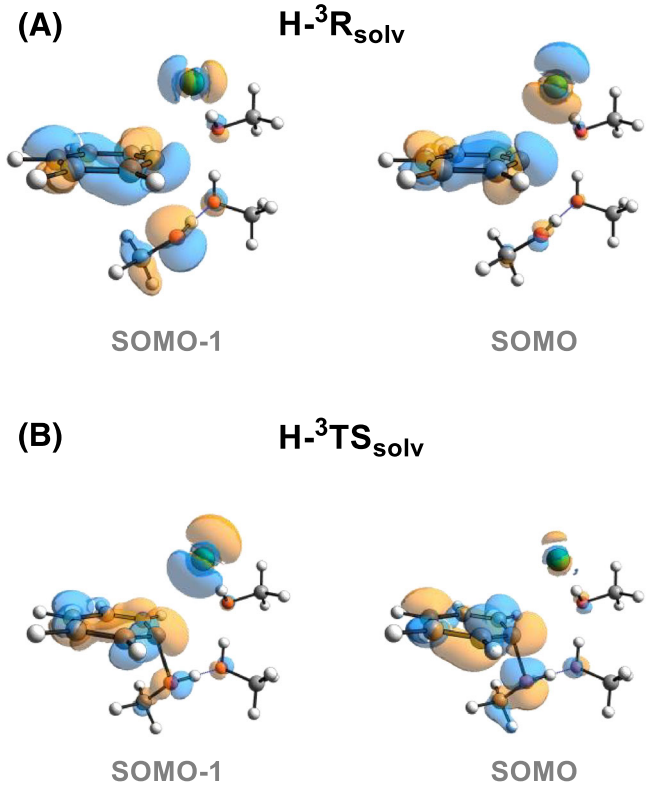

FIGURE 7 Singly occupied molecular orbitals (SOMO and SOMO-1) of the triplet reactants (A) and transition state (B) for the solvolysis of chlorobenzene (isovalue = 0.03, CPCM-(U) PWPBE95-D4/def2-QZVP//r^{2}SCAN-3c)

with the chloride ion. The implicit solvation also has a stabilizing effect on the chloride: in the gas phase **H-^{3}P$_{solv}$** geometry hydrochloric acid is already formed with a −0.38 Cl partial charge (Table S4), while in the CPCM geometry Cl remains as an anion weakly interacting with its environment. Next, the C1 charge decreases in **H-^{3}P$_{solv}$** (0.23), as it gets stabilized by the newly formed C-O bond (1.41 Å). The spin population at C1 suffers only a small drop along the reaction from **H-^{3}R$_{solv}$** (0.97) to **H-^{3}P$_{solv}$** (0.79), which is consistent with a nucleophilic as opposed to a radical attack, giving rise to triplet methoxy-benzene in **H-^{3}P$_{solv}$**.

The C-Cl bond dissociation becomes more advanced in the solvolysis transition state if the compound contains electron donating substituents, with distances of 3.05–3.11 Å for **OMe** and the two conformers of **Si**, or 3.39 Å for **OMe′**. The ring puckering toward O in these **TS$_{solv}$** geometries is also more pronounced ($\alpha = 5.0°$–$8.9°$) and the C-O distances (1.66–1.68 Å) are shorter than in **H-^{3}TS$_{solv}$** (1.71 Å), The negatively charged Cl is weakly interacting with the benzene ring in the transition states of **Si(Z)**, **Si(E)**, **OMe,** and **OMe′**, while in their products it is stabilized by the explicit methanol molecules (vide supra), explaining why the charges on Cl slightly decrease in **^{3}P$_{solv}$**. Nevertheless, the charges and spin populations in the **TS$_{solv}$** structures are comparable to **^{3}P$_{solv}$** and so it can be said that electron donation to the ring pushes the transition state toward a later stage of the reaction.

In parallel to the reduction, placing the –CN group *para* to the chlorine has the opposite effect on the solvolysis transition state. The C-Cl bond of **CN-^{3}TS$_{solv}$** (2.61 Å) is shorter than in **H-^{3}TS$_{solv}$** (2.80 Å) while the ring is flatter ($\alpha = -2.5°$). The electron withdrawing group therefore leads to less C-Cl dissociation in **CN-^{3}TS$_{solv}$** compared to the unsubstituted chlorobenzene case, with a lower Cl partial negative charge (−0.60) and a higher Cl spin population (0.33). The nucleophile is also positioned further away from C1 (1.84 Å), indicating that **CN-^{3}TS$_{solv}$** is an earlier transition state than **H-^{3}TS$_{solv}$**. The cleavage remains heterolytic leading to a chloride anion (−0.82 charge and 0.00 spin) and a triplet *p*-cyano-methoxy-benzene in **CN-^{3}P$_{solv}$** with the spin population delocalized on the benzene ring (Table S5).

The photo-S$_N$2Ar solvolysis via the triplet surface appears thermoneutral for the compounds with electron donating groups (**ΔG_{solv}** = −2.1–2.4 kcal/mol) and slightly exergonic for unsubstituted chlorobenzene (**ΔG_{solv}** = −4.1 kcal/mol). The reaction is most favorable for **CN** (**ΔG_{solv}** = −9.5 kcal/mol), possibly due to the extended conjugation in the product, characterized by a push-pull substitution. In contrast, **CN** encountered the highest activation energy (14.0 kcal/mol), as the electron withdrawing substituent destabilizes the partial positive charge that builds-up on the ring.

Overall, the barriers for the photo-S$_N$2Ar (7.8–14 kcal/mol) are higher than for the radical reduction (4.4–9.9 kcal/mol), but they are still comparable with triplet aryl cation generation. Undissociated triplet chlorobenzenes could therefore also acts as direct precursors for solvolysis products in just one step (Figure 2D), without forming a singlet cation via C-Cl cleavage followed by ISC (Figure 1B). According to the **ΔG** values in Tables 2 and 3, undissociated triplet chlorobenzene and its **Si** and **OMe** derivatives would favor direct hydrogen abstraction from a solvent molecule, which is consistent with experimental product distributions.[15,62] While the generally accepted mechanism attributes the prevalence of photochemical reduction among chlorobenzenes with *para* electron withdrawing substituents to triplet aryl cations, it can be argued that the pathway presented here (Figure 2C) may also play a part due to its low energy barriers.

Interestingly, based on the activation energy of merely 4.4 kcal/mol, one would expect the direct hydrogen abstraction by triplet **OMe′** to outcompete the C-Cl

dissociation/ISC pathway leading to solvolysis (Figure 1E). Experimental yields, however, revealed a 1:2 product ratio between reduction and solvolysis when conducting the reaction in neat methanol.[20] It could be that the presence of the two electron donating groups render the C-Cl dissociation in the triplet state barrierless similarly to *p*-chloroaniline or N,N-dimethyl-*p*-chloroaniline, effectively forming $^{3}\mathbf{Ar}^{+}$ in solution.[28] The greater stability of the singlet cation compared to the triplet in **OMe′-R** could facilitate the ISC even before the triplet reduction.[20]

4 | CONCLUSIONS

Starting from the distorted triplet geometries of chlorobenzene derivatives, we described theoretically alternative pathways to explain excited state reactivities commonly attributed to triplet and singlet aryl cations in polar protic environment. The present results open the possibility for the competing reactions associated with the presence of these intermediates, namely, reduction for $^{3}\mathbf{Ar}^{+}$ and solvolysis for $^{1}\mathbf{Ar}^{+}$, to occur via bimolecular transition states on the same triplet surface of the chloro-derivatives. The calculations matched previous experiments for *para* substituted chlorobenzenes. Energetically, the complete dissociation of the C-Cl bond is therefore not a prerequisite to explain the preferential formation of reduction or solvolysis products, with the reactants and transition states preserving various extents of interaction between the chlorine and the benzene ring.

The difference in Gibbs free energies appears to control the relative feasibilities of the reactions. Electron neutral or donating groups induce reduction over solvolysis, while for electron withdrawing substituents the two processes become comparable in terms of energy barrier and exergonic character.

The extremely low barriers for H-abstraction of **Si** suggest a stepwise mechanism in the reactivity that is associated with the photochemical formation of **DHT** in solution. While the net outcome of the reactivity is unchanged, we propose an alternative interpretation for the photochemical dissociation of **Si**, which involves the H-abstraction from the solvent of the excited chloro-derivative to form the radical cation of the reduced **Si**, which will eventually dissociate to form a benzyl radical. On the other hand, our current picture on the prevalence of solvolysis for *o*-trimethylsilyl-*p*-chloro-anisole **OMe′** appears incomplete. This result could be affected by the increased electron donating character present on the ring, which decreases the barrier for the formation of $^{3}\mathbf{Ar}^{+}$ opening up an alternative pathway to the one we explored in this work. Consequently, more studies are needed to decipher whether the mechanism indeed involves two surfaces (i.e., dissociation in the triplet and solvolysis in the singlet) or just one.

ACKNOWLEDGEMENTS

We thank the Swedish National Infrastructure for Computations (SNIC) for a Small Compute Grant (SNIC 2022/22-525). C. N. thanks Erasmus+ and the Backer foundation at the University of Groningen for mobility grants. S. C. thanks the Swedish Vetenskapsrådet for a Starting Grant (2021-05414).

DATA AVAILABILITY STATEMENT

The data that supports the findings of this study are available in the supplementary material of this article and are openly available in figshare at https://doi.org/10.6084/m9.figshare.20412501.

ORCID

Cristina Nitu https://orcid.org/0000-0003-4728-6985
Stefano Crespi https://orcid.org/0000-0002-0279-4903

REFERENCES

[1] N. C. Baird, *J. Am. Chem. Soc.* **1972**, *94*, 4941.
[2] L. J. Karas, J. I. Wu, *Nat. Chem.* **2022**, *14*, 723.
[3] M. Solà, *Nat. Chem.* **2022**, *14*, 585.
[4] R. Papadakis, H. Ottosson, *Chem. Soc. Rev.* **2015**, *44*, 6472.
[5] E. J. P. Malar, K. Jug, *J. Phys. Chem.* **1984**, *88*, 3508.
[6] M. Baranac-Stojanović, *J. Org. Chem.* **2020**, *85*, 4289.
[7] J. Dreyer, M. Klessinger, *Chem. - A Eur. J.* **1996**, *2*, 335.
[8] T. Slanina, R. Ayub, J. Toldo, J. Sundell, W. Rabten, M. Nicaso, I. Alabugin, I. Fdez, A. K. Galván, R. Gupta, A. Lindh, R. J. Orthaber, G. Lewis, J. Grönberg, H. O. Bergman, *J. Am. Chem. Soc.* **2020**, *142*, 10942.
[9] K. L. Han, G. Z. He, *J. Photochem. Photobiol. C Photochem. Rev.* **2007**, *8*, 55.
[10] M. Fagnoni, A. Albini, *Acc. Chem. Res.* **2005**, *38*, 713.
[11] V. Dichiarante, S. Protti, M. Fagnoni, *J. Photochem. Photobiol. A* **2017**, *339*, 103.
[12] V. Dichiarante, M. Fagnoni, A. Albini, *J. Org. Chem.* **2010**, *75*, 1271.
[13] S. Lazzaroni, D. Dondi, M. Fagnoni, A. Albini, *J. Org. Chem.* **2010**, *75*, 315.
[14] D. Ravelli, S. Protti, M. Fagnoni, A. Albini, *J. Org. Chem.* **2013**, *78*, 3814.
[15] C. Pedroli, D. Ravelli, S. Protti, A. Albini, M. Fagnoni, *J. Org. Chem.* **2017**, *82*, 6592.
[16] S. Crespi, S. Protti, D. Ravelli, D. Merli, M. Fagnoni, *J. Org. Chem.* **2017**, *82*, 12162.
[17] M. Abe, *Chem. Rev.* **2013**, *113*, 7011.
[18] S. Crespi, D. Ravelli, S. Protti, A. Albini, M. Fagnoni, *Chem. A Eur. J.* **2014**, *20*, 17572.
[19] S. Protti, D. Ravelli, B. Mannucci, A. Albini, M. Fagnoni, *Angew. Chem. Int. Ed.* **2012**, *51*, 8577.
[20] V. Dichiarante, A. Salvaneschi, S. Protti, D. Dondi, M. Fagnoni, A. Albini, *J. Am. Chem. Soc.* **2007**, *129*, 15919.

[21] S. M. Gasper, G. B. Schuster, C. Devadoss, *J. Am. Chem. Soc.* **1995**, *117*, 5206.
[22] S. Bonesi, S. Protti, M. Fagnoni, *Chem. - A Eur. J.* **2021**, *27*, 6315.
[23] I. Manet, S. Monti, G. Grabner, S. Protti, D. Dondi, V. Dichiarante, M. Fagnoni, A. Albini, *Chem. - A Eur. J.* **2008**, *14*, 1029.
[24] S. Lazzaroni, D. Dondi, M. Fagnoni, A. Albini, *J. Org. Chem.* **2008**, *73*, 206.
[25] D. Ravelli, S. Protti, M. Fagnoni, *J. Org. Chem.* **2015**, *80*, 852.
[26] K. K. Laali, G. Rasul, G. K. S. Prakash, G. A. Olah, *J. Org. Chem.* **2002**, *67*, 2913.
[27] M. Freccero, M. Fagnoni, A. Albini, *J. Am. Chem. Soc.* **2003**, *125*, 13182.
[28] C. Raviola, D. Ravelli, S. Protti, A. Albini, M. Fagnoni, *Synlett* **2015**, *26*, 471.
[29] L. Zhang, E. M. Israel, J. Yan, T. Ritter, *Nat. Synth.* **2022**, *1*, 376.
[30] F. Neese, F. Wennmohs, U. Becker, C. Riplinger, *J. Chem. Phys.* **2020**, *152*, 224108.
[31] F. Neese, *Wiley Interdiscip. Rev: Comput. Mol. Sci.* **2022**, *12*. PMID: e1606.
[32] C. Bannwarth, E. Caldeweyher, S. Ehlert, A. Hansen, P. Pracht, J. Seibert, S. Spicher, S. Grimme, *Wiley Interdiscip. Rev. Comput. Mol. Sci.* **2021**, *11*, e1493.
[33] C. Bannwarth, S. Ehlert, S. Grimme, *J. Chem. Theory Comput.* **2019**, *15*, 1652.
[34] S. Grimme, *J. Chem. Theory Comput.* **2019**, *15*, 2847.
[35] P. Pracht, F. Bohle, S. Grimme, *Phys. Chem. Chem. Phys.* **2020**, *22*, 7169.
[36] S. Spicher, C. Plett, P. Pracht, A. Hansen, S. Grimme, *J. Chem. Theory Comput.* **2022**, *18*, 3174.
[37] V. Barone, M. Cossi, *J. Phys. Chem. A* **1998**, *102*, 1995.
[38] F. Aquilante, J. Autschbach, A. Baiardi, S. Battaglia, V. A. Borin, L. F. Chibotaru, I. Conti, L. De Vico, M. Delcey, I. F. Galván, N. Ferré, L. Freitag, M. Garavelli, X. Gong, S. Knecht, E. D. Larsson, R. Lindh, M. Lundberg, P. Å. Malmqvist, A. Nenov, J. Norell, M. Odelius, M. Olivucci, T. B. Pedersen, L. Pedraza-González, Q. M. Phung, K. Pierloot, M. Reiher, I. Schapiro, J. Segarra-Martí, F. Segatta, L. Seijo, S. Sen, D. C. Sergentu, C. J. Stein, L. Ungur, M. Vacher, A. Valentini, V. Veryazov, *J. Chem. Phys.* **2020**, *152*, 214117.
[39] I. Fdez, M. Galván, A. Vacher, C. Alavi, F. Angeli, J. Aquilante, J. J. Autschbach, S. I. Bao, N. A. Bokarev, R. K. Bogdanov, L. F. Carlson, J. Chibotaru, N. Creutzberg, M. G. Dattani, S. S. Delcey, A. Dong, L. Dreuw, L. M. Freitag, L. Frutos, F. Gagliardi, A. Gendron, L. Giussani, G. González, M. Grell, C. E. Guo, M. Hoyer, S. Johansson, S. Keller, G. Knecht, E. Kovačević, G. L. Källman, M. Manni, Y. Lundberg, S. Ma, J. P. Mai, P. Å. Malhado, P. Malmqvist, S. A. Marquetand, J. Mewes, M. Norell, M. Olivucci, Q. M. Oppel, K. Phung, F. Pierloot, M. Plasser, A. M. Reiher, I. Sand, P. Schapiro, C. J. Sharma, L. K. Stein, D. G. Sørensen, M. Truhlar, L. Ugandi, A. Ungur, S. Valentini, V. Vancoillie, O. Veryazov, T. A. Weser, P. O. Wesołowski, S. Widmark, A. Wouters, J. P. Zech, R. L. Zobel, *J. Chem. Theory Comput.* **2019**, *15*, 5925.
[40] E. D. Glendening, C. R. Landis, F. Weinhold, *J. Comput. Chem.* **2013**, *34*, 1429.
[41] A. D. Becke, *Phys. Rev. A* **1988**, *38*, 3098.
[42] A. D. Becke, *J. Chem. Phys.* **1993**, *98*, 5648.
[43] R. Krishnan, J. S. Binkley, R. Seeger, J. A. Pople, *J. Chem. Phys.* **1980**, *72*, 650.
[44] F. Weigend, R. Ahlrichs, *Phys. Chem. Chem. Phys.* **2005**, *7*, 3297.
[45] F. Weigend, *Phys. Chem. Chem. Phys.* **2006**, *8*, 1057.
[46] Y. Zhao, D. G. Truhlar, *Theor Chem Account* **2008**, *120*, 215.
[47] S. Grimme, J. Antony, S. Ehrlich, H. Krieg, *J. Chem. Phys.* **2010**, *132*, 154104.
[48] S. Grimme, A. Hansen, S. Ehlert, J. M. Mewes, *J. Chem. Phys.* **2021**, *154*, 064103.
[49] B. O. Roos, P. R. Taylor, P. E. M. Sigbahn, *Chem. Phys.* **1980**, *48*, 157.
[50] B. O. Roos, *AB Initio Methods Quantum Chem.-II* **2007**, *69*, 399.
[51] Y. Zhao, D. G. Truhlar, *J. Phys. Chem. A* **2005**, *109*, 5656.
[52] E. Caldeweyher, C. Bannwarth, S. Grimme, *J. Chem. Phys.* **2017**, *147*, 034112.
[53] J. R. Pliego, J. M. Riveros, *J. Phys. Chem. A* **2001**, *105*, 7241.
[54] L. Di Terlizzi, F. Roncari, S. Crespi, S. Protti, M. Fagnoni, *Photochem. Photobiol. Sci.* **2022**, *21*, 667.
[55] C. Raviola, F. Chiesa, S. Protti, A. Albini, M. Fagnoni, *J. Org. Chem.* **2016**, *81*, 6336.
[56] M. S. Lenczewski, H. J. P. De Lijser, D. M. Turner, J. P. Dinnocenzo, *J. Org. Chem.* **2017**, *82*, 12112.
[57] A. Cantos, J. Marauet, M. Moreno-Mañas, A. González-Lafont, J. M. Lluch, J. Bertran, *J. Org. Chem.* **1990**, *55*, 3303.
[58] G. G. Wubbels, *Tetrahedron Lett.* **2014**, *55*, 5066.
[59] G. G. Wubbels, T. R. Brown, T. A. Babcock, K. M. Johnson, *J. Org. Chem.* **2008**, *73*, 1925.
[60] H. C. H. A. Van Riel, G. Lodder, E. Havinga, *J. Am. Chem. Soc.* **1981**, *103*, 7257.
[61] C. Karapire, S. Icli, in *CRC Handbook of Organic Photochemistry and Photobiology*, 2nd ed. (Eds: W. Horspool, F. Lenci), CRC PRESS LLC **2004**.
[62] S. Protti, M. Fagnoni, M. Mella, A. Albini, *J. Org. Chem.* **2004**, *69*, 3465.

SUPPORTING INFORMATION

Additional supporting information can be found online in the Supporting Information section at the end of this article.

How to cite this article: C. Nitu, S. Crespi, *J Phys Org Chem* **2023**, *36*(1), e4437. https://doi.org/10.1002/poc.4437